



Dalton  
Transactions

**An Organometallic Catalase Mimic with Exceptional Activity,  
H<sub>2</sub>O<sub>2</sub> Stability, and Catalase/Peroxidase Selectivity**

Journal:	<i>Dalton Transactions</i>
Manuscript ID	DT-ART-06-2021-002002.R1
Article Type:	Paper
Date Submitted by the Author:	21-Aug-2021
Complete List of Authors:	Lu, Zhuomin; 219 H.L. Hunter Chem. Laboratory, Chemistry; Shantou University, Chemistry Lightcap, Ian; University of Notre Dame, Center for Sustainable Energy Tennyson, Andrew; Clemson University, Department of Chemistry

SCHOLARONE™  
Manuscripts

## An Organometallic Catalase Mimic with Exceptional Activity, H<sub>2</sub>O<sub>2</sub> Stability, and Catalase/Peroxidase Selectivity

Zhuomin Lu,<sup>a</sup> Ian V. Lightcap,<sup>b</sup> and Andrew G. Tennyson\*<sup>†a,c,d</sup>

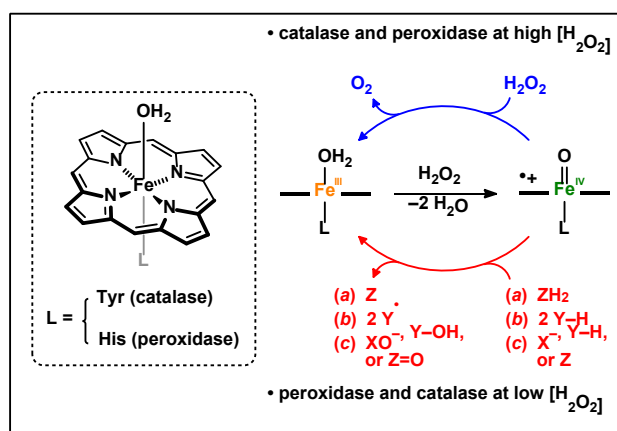
Received 00th January 20xx,  
Accepted 00th January 20xx

DOI: 10.1039/x0xx00000x

Manganese–porphyrin and –salen redox therapeutics catalyze redox reactions involving O<sub>2</sub><sup>•−</sup>, H<sub>2</sub>O<sub>2</sub>, and other reactive oxygen species, thereby modulating cellular redox states. Many of these complexes perform catalase reactions via high-valent Mn–oxo or –hydroxo intermediates that oxidize H<sub>2</sub>O<sub>2</sub> to O<sub>2</sub>, but these intermediates can also oxidize other molecules (e.g., thiols), which is peroxidase reactivity. Whether catalase or peroxidase reactivity predominates depends on the metal–ligand set and the local environment, complicating predictions of what therapeutic effects (e.g., promoting vs. suppressing apoptosis) a complex might produce in a given disease. We recently reported an organoruthenium complex (**Ru1**) that catalyzes ABTS<sup>•+</sup> reduction to ABTS<sup>2−</sup> with H<sub>2</sub>O<sub>2</sub> as the terminal reductant. Given that H<sub>2</sub>O<sub>2</sub> is thermodynamically a stronger oxidant than ABTS<sup>•+</sup>, we reasoned that the intermediate that reduced ABTS<sup>•+</sup> would also be able to reduce H<sub>2</sub>O<sub>2</sub> to H<sub>2</sub>O. Herein we demonstrate **Ru1**-catalyzed H<sub>2</sub>O<sub>2</sub> disproportionation into O<sub>2</sub> and H<sub>2</sub>O, exhibiting an 8,580-fold faster catalase TOF vs. peroxidase TOF, which is 89.2-fold greater than the highest value reported for a Mn-porphyrin or –salen complex. Furthermore, **Ru1** was 120-fold more stable to H<sub>2</sub>O<sub>2</sub> than the best MnSOD mimic (TON = 4000 vs. 33.4). Mechanistic studies provide evidence that the mechanism for **Ru1**-catalyzed H<sub>2</sub>O<sub>2</sub> disproportionation is conserved with the mechanism for ABTS<sup>•+</sup> reduction. Therapeutic effects of redox catalysts can be predicted with greater accuracy for catalysts that exhibit exclusively catalase activity, thereby facilitating the development of future redox therapeutic strategies for diseases.

### Introduction

Catalases are metalloenzymes that catalyze the disproportionation of H<sub>2</sub>O<sub>2</sub> into H<sub>2</sub>O and ½ O<sub>2</sub>,<sup>1</sup> whereas peroxidases catalyze the reduction of H<sub>2</sub>O<sub>2</sub> into H<sub>2</sub>O via oxidation of other substrates.<sup>2</sup> In both enzyme classes, H<sub>2</sub>O<sub>2</sub> is reduced to H<sub>2</sub>O and the Fe(III) enzyme resting state is oxidized to an O=Fe(IV)–porphyrin<sup>•+</sup> intermediate (Scheme 1). In a catalase, this intermediate oxidizes a 2<sup>nd</sup> equivalent of H<sub>2</sub>O<sub>2</sub> to O<sub>2</sub>, releasing a 2<sup>nd</sup> equivalent of H<sub>2</sub>O and regenerating the Fe(III) resting state. In a peroxidase, however, this intermediate oxidizes a substrate other than H<sub>2</sub>O<sub>2</sub>,<sup>3</sup> proceeding via (a) 2e<sup>−</sup> oxidation of one substrate molecule,<sup>4, 5</sup> (b) 1e<sup>−</sup> oxidation of two substrate molecules,<sup>6, 7</sup> or (c) oxygen atom transfer to a substrate molecule.<sup>8–11</sup> Given the similarity between the O=Fe(IV)–porphyrin<sup>•+</sup> intermediates in catalase and peroxidase, it is unsurprising that catalase can exhibit peroxidase reactivity at a sufficiently low [H<sub>2</sub>O<sub>2</sub>],<sup>12</sup> or that peroxidase can exhibit catalase reactivity at sufficiently high [H<sub>2</sub>O<sub>2</sub>].<sup>13</sup>



Scheme 1. Dual catalase / peroxidase activity from a common intermediate

Synthetic Mn complexes supported by porphyrin and salen ligands, designed as manganese superoxide dismutase (MnSOD) mimics, catalyze the disproportionation of O<sub>2</sub><sup>•−</sup> into O<sub>2</sub> and H<sub>2</sub>O<sub>2</sub>.<sup>14–19</sup> However, these Mn-porphyrin and –salen complexes also catalyze the disproportionation of H<sub>2</sub>O<sub>2</sub> into H<sub>2</sub>O and ½ O<sub>2</sub>,<sup>19, 20</sup> which is unsurprising given that a Mn complex able to reduce O<sub>2</sub> to O<sub>2</sub><sup>•−</sup> (E<sub>0</sub>' = −0.33 V vs. NHE)<sup>21</sup> will likewise be able to reduce H<sub>2</sub>O<sub>2</sub> to 2 H<sub>2</sub>O (E<sub>0</sub>' = −1.35 V).<sup>22</sup> Because the latter reduction is more thermodynamically favorable, many of the Mn-porphyrin and –salen complexes that are capable of MnSOD activity are also intrinsically capable of catalase activity.

<sup>a</sup> Department of Chemistry, Clemson University, Clemson University.

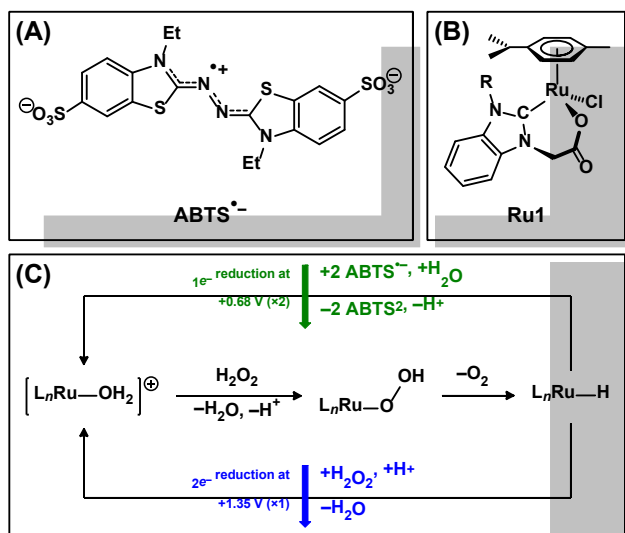
<sup>b</sup> Center for Sustainable Energy, University of Notre Dame, Notre Dame, IN 46556.

<sup>c</sup> Department of Materials Science and Engineering, Clemson University, Clemson, SC 29634.

<sup>d</sup> Department of Chemistry, National Sun Yat-sen University, Kaohsiung 80424, Taiwan

<sup>†</sup> NRC Senior Research Fellowship address: Chemistry Research Center, United States Air Force Academy, USAF Academy, CO 80840

Electronic Supplementary Information (ESI) available: Details of experimental procedures, rate law equation derivations, and additional kinetics plots. See DOI: 10.1039/x0xx00000x



**Scheme 2.** Structure of (A) ABTS<sup>•-</sup> and (B) Ru1. (C) Rationale that H<sub>2</sub>O<sub>2</sub> disproportionation can be catalyzed by Ru1 via the same intermediates that form during ABTS<sup>•-</sup> reduction.

As is observed with catalase itself, some Mn–salen and Mn–porphyrin complexes that (a) exhibit catalase activity can also (b) exhibit peroxidase activity,<sup>23, 24</sup> such as oxidizing ABTS<sup>2-</sup> to ABTS<sup>•-</sup> (Scheme 2A).<sup>25–32</sup> Even non-biomimetic Mn complexes will toggle between catalase activity<sup>33</sup> vs. peroxidase activity<sup>34</sup> upon simple ligand modification (e.g., R = Me vs. *t*-Bu). Thus, a single Mn complex is capable of producing either antioxidant or pro-oxidant effects in a given biological environment, with its behavior being determined by the metal–ligand set and the local conditions. For example, the Mn–porphyrin complexes that have entered clinical trials can (i) promote cancer cell death by shifting cellular redox states to more oxidized potentials,<sup>35, 36</sup> or (ii) promote normal cell survival during radiotherapy by shifting cellular redox states to more reduced potentials.<sup>37, 38</sup> Both outcomes are highly beneficial to patients and illustrate the enormous therapeutic potential for complexes capable of both catalase and peroxidase activity. However, it is difficult to predict in advance which reactivity mode will predominate in a given biological environment.

Our lab developed an organoruthenium complex (Ru1, Scheme 2B) that can catalytically reduce ABTS<sup>•-</sup> to ABTS<sup>2-</sup> by oxidizing biologically-relevant alcohols as the terminal reductants.<sup>39–41</sup> We recently demonstrated that Ru1 can also harness H<sub>2</sub>O<sub>2</sub> as the terminal reductant, generating O<sub>2</sub>(g) and a Ru–H intermediate, the latter then reducing 2 equiv. of ABTS<sup>•-</sup> to ABTS<sup>2-</sup> (Scheme 2C, top).<sup>42</sup> Because the ABTS<sup>•-</sup>/ABTS<sup>2-</sup> redox couple occurs at +0.68 V,<sup>43</sup> and the standard reduction potential for H<sub>2</sub>O<sub>2</sub> to 2 H<sub>2</sub>O is much higher (+1.35 V),<sup>22</sup> we reasoned that a Ru1-derived intermediate capable of reducing 2 ABTS<sup>•-</sup> to 2 ABTS<sup>2-</sup> will also be capable of reducing the more strongly-oxidizing H<sub>2</sub>O<sub>2</sub> to 2 H<sub>2</sub>O, thus exhibiting catalase activity (Scheme 2C, bottom). Moreover, given that Ru1 can use H<sub>2</sub>O<sub>2</sub> to reduce ABTS<sup>•-</sup> to ABTS<sup>2-</sup>, we reasoned that Ru1 would show little to no oxidation of ABTS<sup>2-</sup> to ABTS<sup>•-</sup> with H<sub>2</sub>O<sub>2</sub>, with this latter reaction being a spectroscopically-convenient probe for peroxidase reactivity.

Herein we report the catalytic disproportionation of H<sub>2</sub>O<sub>2</sub> into H<sub>2</sub>O and ½ O<sub>2</sub> by Ru1 with values for catalase TOF = 1.09 s<sup>-1</sup>, catalase TON ≥ 4000, and catalase/peroxidase selectivity = 8,580, which are individually 11.9-, 120-, and 89.2-fold greater, respectively, than the highest values reported<sup>44</sup> for the Mn–porphyrin and Mn–salen MnSOD mimics.<sup>19, 20, 23–32</sup> Using a combination of catalase TOF, catalase TON, and catalase/peroxidase selectivity values, the aggregated functionality of Ru1 as a catalase mimic is 14,200-fold higher than the best-performing synthetic MnSOD mimic.

## Results and Discussion

### Catalase and peroxidase reactivity

Addition of 20 mM H<sub>2</sub>O<sub>2</sub> to a solution of 20 μM Ru1 in 3.00 mL PBS (pH 7.4, 25 °C) results in a gradual decrease in the absorbance at 240 nm ( $\epsilon_{240} = 43.6 \text{ M}^{-1}\text{cm}^{-1}$  for H<sub>2</sub>O<sub>2</sub>) that is complete within 2 h (Figure 1, blue trace). The  $v_0$  measured is  $17.1 \pm 1.0 \mu\text{M s}^{-1}$ ,<sup>45</sup> corresponding to a catalase TOF =  $0.868 \pm 0.063 \text{ s}^{-1}$ .<sup>46, 47</sup> When this experiment is repeated on a 100 mL scale, to facilitate quantification of O<sub>2</sub>(g) evolution, 1.04 ± 0.02 mmol of O<sub>2</sub>(g) is collected, corresponding to a TON = 1000 and in good agreement with the 25 mL theoretical volume if every 1.0 equivalent of H<sub>2</sub>O<sub>2</sub> that was consumed produced 0.5 equiv. of O<sub>2</sub>(g). Four successive 20 mM aliquots of H<sub>2</sub>O<sub>2</sub> added every 2 h are all completely consumed by 20 μM Ru1 in PBS, yielding a minimum catalase TON = 4000 for Ru1. Headspace gas sampling to a thermocouple detector confirms that 100% of the evolved gas was O<sub>2</sub>(g). In situ mass spectrometric analysis of these H<sub>2</sub>O<sub>2</sub> disproportionation reactions reveals the same intermediates as those in Ru1-catalyzed ABTS<sup>•-</sup> reduction with H<sub>2</sub>O<sub>2</sub>.<sup>42</sup>

To assess potential peroxidase activity of Ru1, 100 μM ABTS<sup>2-</sup> is introduced to a PBS solution containing 20 μM Ru1 followed by the addition of 5 μM H<sub>2</sub>O<sub>2</sub>. The 4:1 Ru1/H<sub>2</sub>O<sub>2</sub> ratio is chosen to maximize coordination of H<sub>2</sub>O<sub>2</sub> to Ru1 and minimize the amount of free H<sub>2</sub>O<sub>2</sub> in solution available to undergo disproportionation by any Ru1/H<sub>2</sub>O<sub>2</sub> derived species. The 20:1 ABTS<sup>2-</sup>/H<sub>2</sub>O<sub>2</sub> ratio was selected such that any Ru1/H<sub>2</sub>O<sub>2</sub> derived species would be significantly more likely to encounter ABTS<sup>2-</sup> than H<sub>2</sub>O<sub>2</sub>, thus favoring oxidation of ABTS<sup>2-</sup> (peroxidase reactivity) over disproportionation of H<sub>2</sub>O<sub>2</sub> (catalase reactivity).

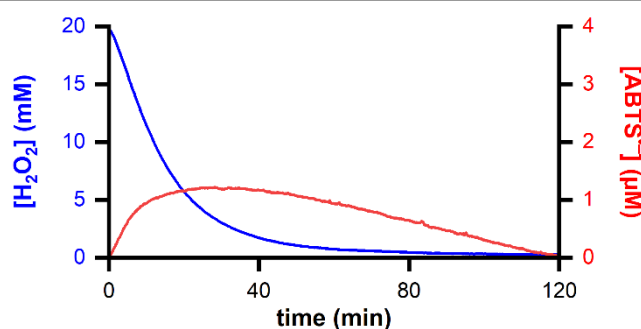


**Figure 1.** Plot of concentration vs. time for H<sub>2</sub>O<sub>2</sub> disproportionation (blue trace) and ABTS<sup>2-</sup> oxidation (red trace) catalyzed by Ru1. Conditions: [H<sub>2</sub>O<sub>2</sub>]<sub>0</sub> = 20 mM (blue trace) or 5 μM (red trace), [ABTS<sup>2-</sup>]<sub>0</sub> = 0 μM (blue trace) or 200 μM (red trace), [Ru1]<sub>0</sub> = 20 μM, PBS (pH 7.4), 25 °C.

When 5  $\mu\text{M}$   $\text{H}_2\text{O}_2$  is added to a solution of 20  $\mu\text{M}$  **Ru1** and 100  $\mu\text{M}$   $\text{ABTS}^{2-}$  in PBS, the absorbance at 734 nm (characteristic for  $\text{ABTS}^{+}$ )<sup>48</sup> gradually increases, reaching a maximum of  $1.69 \pm 0.13 \mu\text{M}$  after 28 min, and then gradually decays to zero over the course of 2 h (Figure 1, red trace). The  $v_0$  measured is  $2.54 \pm 0.03 \text{ nM s}^{-1}$ , corresponding to a peroxidase TOF =  $1.27 \pm 0.01 \times 10^{-4} \text{ s}^{-1}$ . Dividing the catalase TOF by the peroxidase TOF yields the catalase/peroxidase selectivity ratio (C/P), which for **Ru1** (at 20  $\mu\text{M}$ ) is 6,830. Notably, 5  $\mu\text{M}$   $\text{H}_2\text{O}_2$  should have been sufficient to oxidize 10  $\mu\text{M}$   $\text{ABTS}^{2-}$  to 10  $\mu\text{M}$   $\text{ABTS}^{+}$ , but a maximum of only  $1.69 \pm 0.13 \mu\text{M}$   $\text{ABTS}^{+}$  forms under these conditions, which demonstrates that only 17% of the total  $\text{H}_2\text{O}_2$  is consumed by peroxidase reactivity, and the remaining 83% is consumed by catalase reactivity.

Catalase and peroxidase activities of **Ru1** were measured again at 10  $\mu\text{M}$  to match the concentrations employed in studies of Mn-based catalase mimics. At  $[\text{Ru1}]_0 = 10 \mu\text{M}$ , the catalase and peroxidase  $v_0$  values are  $10.6 \pm 0.5 \mu\text{M s}^{-1}$  and  $1.27 \pm 0.12 \text{ nM s}^{-1}$ , respectively (Figure S1), corresponding to a catalase TOF =  $1.09 \pm 0.13 \text{ s}^{-1}$ , a peroxidase TOF =  $1.27 \pm 0.12 \times$

$10^{-4} \text{ s}^{-1}$ , and a C/P = 8,580 (Table 1). For comparison, **MnP-1** (Figure 2) has the highest catalase activity (TOF =  $9.14 \times 10^{-2} \text{ s}^{-1}$ )<sup>20</sup> of the porphyrin-based MnSOD mimics, which is 11.9-fold lower than **Ru1**. The highest catalase TON value achieved is 25.1 with **MnP-2**, 159-fold lower than **Ru1**. Using oxidation of  $\text{ABTS}^{2-}$  to  $\text{ABTS}^{+}$  as the measure of peroxidase activity, **MnP-3** exhibited the highest catalase/peroxidase selectivity (C/P = 96.2),<sup>30</sup> which is 89.2-fold lower than **Ru1**.

Among the salen-based MnSOD mimics,<sup>49</sup> **MnS-1** has the highest reported catalase TOF ( $5.87 \times 10^{-2} \text{ s}^{-1}$ ),<sup>32</sup> which is 18.6-fold lower than **Ru1**. The highest catalase TON is 33.4 for **MnS-2**, 120-fold lower than **Ru1**. The best catalase selectivity among the Mn-salen MnSOD mimics is observed with **MnS-3** (C/P = 9.16), which is 937-fold lower than **Ru1**. Porphyrin- and salen-based MnSOD mimics have been reported to exhibit perfect catalase selectivity (i.e., zero peroxidase activity with nonzero catalase activity),<sup>29, 32</sup> but they suffer from poor  $\text{H}_2\text{O}_2$  stability (TON < 3), which could indicate that the observed catalase reactivity is non-catalytic.

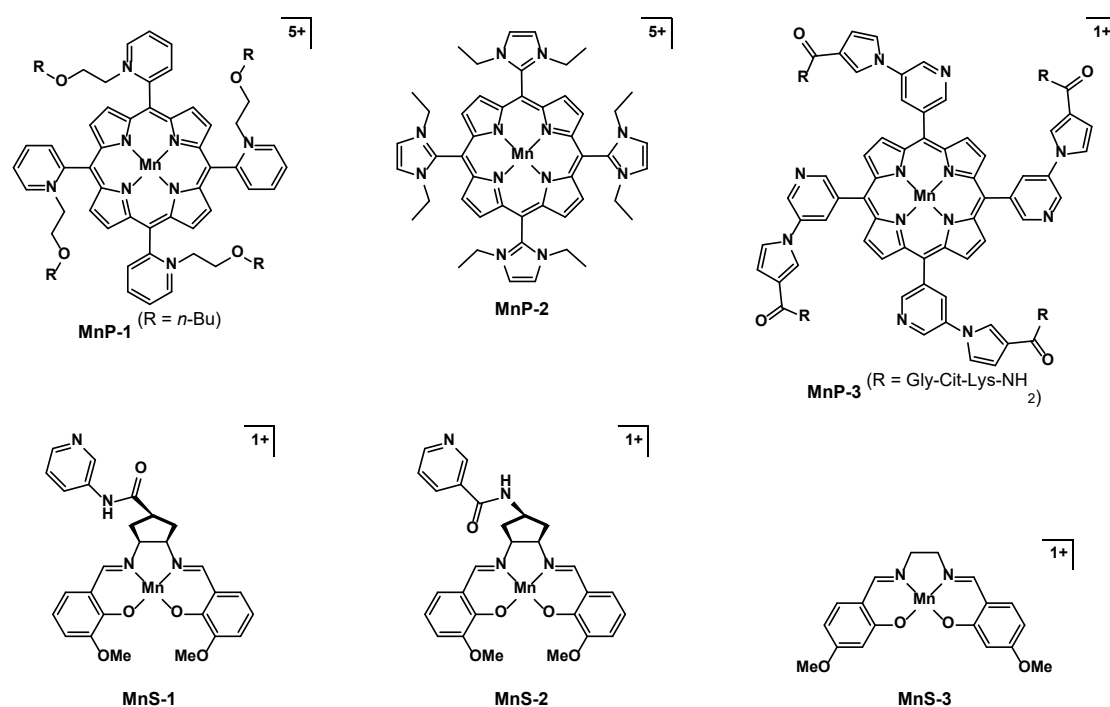
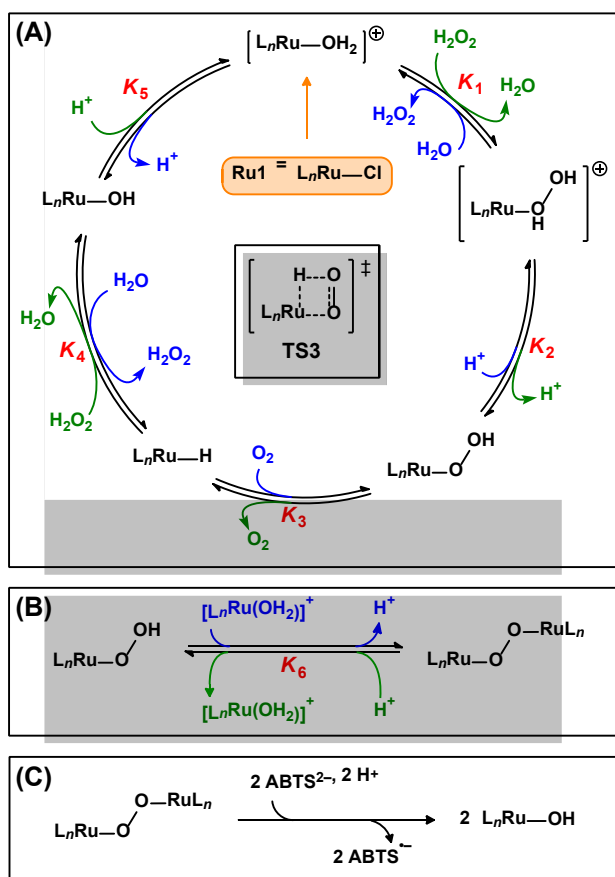


Figure 2. Best-performing Mn-porphyrin (**MnP**) and Mn-salen (**MnS**) catalase mimics. The 5<sup>th</sup> ligands (Cl or OAc) for **MnS** have been omitted for clarity.

Table 1. Comparison of catalase and peroxidase kinetic parameters for **Ru1** to porphyrin- and salen-based MnSOD mimics **MnP** and **MnS**

	catalase TOF ( $\text{s}^{-1}$ )	catalase TON	peroxidase TOF ( $\text{s}^{-1}$ )	C/P selectivity	CCN	CPCN	Reference
<b>Ru1</b>	1.09	$\geq 4000$	$1.27 \times 10^{-4}$	$8.58 \times 10^3$	$4.36 \times 10^3$	$3.43 \times 10^7$	this work
<b>MnP-1</b>	$9.14 \times 10^{-2}$	18.0	—	—	1.65	<sup>a</sup> $1.73 \times 10^3$	20
<b>MnP-2</b>	$2.92 \times 10^{-2}$	25.1	—	—	0.733	<sup>a</sup> $2.41 \times 10^3$	20
<b>MnP-3</b>	$2.00 \times 10^{-2}$	19.4	$2.08 \times 10^{-4}$	96.2	0.388	$1.87 \times 10^3$	30
<b>MnS-1</b>	$5.87 \times 10^{-2}$	28.8	$1.23 \times 10^{-2}$	4.77	1.69	137	27
<b>MnS-2</b>	$5.69 \times 10^{-2}$	33.4	$1.49 \times 10^{-2}$	3.82	1.90	128	27
<b>MnS-3</b>	$6.11 \times 10^{-3}$	2.4	$6.67 \times 10^{-4}$	9.16	$1.47 \times 10^{-2}$	22.0	32

(a) Calculated by assigning to **MnP-1** and **MnP-2** a C/P selectivity value equal to that for **MnP-3**.



**Scheme 3.** Proposed mechanisms for (A) **Ru1**-catalyzed H<sub>2</sub>O<sub>2</sub> disproportionation, (B) formation of a bimetallic intermediate that would cause non-linear behaviour in the  $v_0$  vs.  $[\mathbf{Ru1}]_0$  plot, and (C) reaction of a bimetallic peroxo intermediate with ABTS<sup>2-</sup> that would cause ABTS<sup>-</sup> formation without permanent catalyst deactivation.

The catalase activity, H<sub>2</sub>O<sub>2</sub> stability, and catalase/peroxidase selectivity values for **Ru1** are each greater than the highest *individual value* among the MnSOD mimics (11.9-, 120-, and 89.2-fold greater, respectively). However, this understates the performance of **Ru1** as a whole relative to each *individual Mn complex in its totality*. If we define a "catalase comparison number" (CCN) as catalase TOF × catalase TON, the CCN for **Ru1** (4,360) is 2,290-fold higher than the best-performing Mn-based complex **MnS-2** (CCN = 1.90). If we divide CCN by peroxidase TOF to account for any competing peroxidase activity, i.e., CPCN = catalase TON × C/P, the CPCN for **Ru1** ( $3.75 \times 10^7$ ) is 14,200-fold higher than for **MnP-2** (CPCN =  $2.41 \times 10^3$ ). Thus, not only are each individual catalase activity, H<sub>2</sub>O<sub>2</sub> stability, and C/P value for **Ru1** greater than the highest reported values for Mn-porphyrin and -salen MnSOD mimics by 1-2 orders of magnitude, the overall catalase performance of **Ru1** as a whole is 3-4 orders of magnitude greater than the best-performing MnSOD mimics.

### Proposed mechanism

We envision a mechanism for **Ru1**-catalyzed H<sub>2</sub>O<sub>2</sub> disproportionation (Scheme 3A) that is conserved with the previously-established mechanism for **Ru1**-catalyzed ABTS<sup>-</sup>

reduction with H<sub>2</sub>O<sub>2</sub>. Addition of **Ru1** to an aqueous PBS solution will result in rapid exchange between Cl and H<sub>2</sub>O, initiating the catalytic cycle by forming the aquo complex [L<sub>n</sub>Ru(OH<sub>2</sub>)]<sup>1+</sup>. Loss of H<sub>2</sub>O and coordination of H<sub>2</sub>O<sub>2</sub> will yield [L<sub>n</sub>Ru(H<sub>2</sub>O<sub>2</sub>)]<sup>1+</sup> (step 1) and subsequent H<sup>+</sup> dissociation to the buffered aqueous solution will afford the hydroperoxo complex [L<sub>n</sub>Ru(OOH)]<sup>+</sup> (step 2). We hypothesize that fragmentation of the hydroperoxo ligand will release O<sub>2</sub>(g) and the resulting 2e<sup>-</sup> will be transferred to the [L<sub>n</sub>Ru] core, along with the hydrogen, to generate [L<sub>n</sub>Ru-H] (step 3). Alternatively, the H-atom could transfer to the ligand CO<sub>2</sub><sup>-</sup> group as H<sup>+</sup>, leaving behind an O<sub>2</sub> ligand on a Ru center with an oxidation state of 0, 1+, 2+, depending on the O<sub>2</sub> binding mode. Independent of the structure of this intermediate, the key to the exceptional H<sub>2</sub>O<sub>2</sub> stability and catalase/peroxidase selectivity of **Ru1** is the fact that the 1<sup>st</sup> equivalent of H<sub>2</sub>O<sub>2</sub> functions as a reductant. The Ru-H intermediate, or some other **Ru1**-derived species reduced by H<sub>2</sub>O<sub>2</sub>, will then be oxidized by the 2<sup>nd</sup> equivalent of H<sub>2</sub>O<sub>2</sub>, which affords H<sub>2</sub>O and HO<sup>-</sup>, with HO<sup>-</sup> remaining coordinated to the metal in [L<sub>n</sub>Ru-OH] (step 4). This hydroxo complex will then acquire an H<sup>+</sup> from solution to regenerate [L<sub>n</sub>Ru(OH<sub>2</sub>)]<sup>1+</sup> (step 5) and thereby restart the catalytic cycle.

If the proposed mechanism in Scheme 3A completely describes all aspects of **Ru1**-catalyzed H<sub>2</sub>O<sub>2</sub> reduction, then the fact that all proposed Ru-containing intermediates are mononuclear will require the initial rate ( $v_0$ ) of **Ru1**-catalyzed H<sub>2</sub>O<sub>2</sub> reduction to be first order in  $[\mathbf{Ru1}]_0$ . Although a plot of  $v_0$  vs.  $[\mathbf{Ru1}]_0$  can be fit by a linear equation (Figure S2A), the y-intercept corresponds to an uncatalyzed H<sub>2</sub>O<sub>2</sub> degradation rate of 5 μM s<sup>-1</sup>, which is too high by many orders of magnitude. Forcing the linear equation to have a y-intercept of zero results in a poor match between the fit and data (Figure S2B).

We reasoned that dimerization of a Ru-containing species can potentially, and reversibly, generate a catalytically-incompetent intermediate, where (a) low  $[\mathbf{Ru1}]_0$  leads to negligible dimer formation and thus  $v_0$  will increase with  $[\mathbf{Ru1}]_0$  in 1:1 fashion, but then (b) high  $[\mathbf{Ru1}]_0$  leads to significant dimer formation and  $v_0$  will thus increase with  $[\mathbf{Ru1}]_0$  in less than 1:1 fashion. We propose  $[\{\text{L}_n\text{Ru}\}_2(\mu_{1,2}\text{-O}_2)]$  as the most likely bimetallic intermediate, which would be formed via reaction of [L<sub>n</sub>Ru(OOH)] with [L<sub>n</sub>Ru(OH<sub>2</sub>)]<sup>1+</sup> (Scheme 3B).

Although [L<sub>n</sub>Ru(OH<sub>2</sub>)]<sup>1+</sup> could itself dimerize to generate species such as  $[\{\text{L}_n\text{Ru}\}_2(\mu\text{-OH})]^{1+}$  or  $[\{\text{L}_n\text{Ru}\}_2(\mu\text{-O})]$ , we believe the 1000-fold excess of H<sub>2</sub>O<sub>2</sub> relative to **Ru1** results in the concentration of [L<sub>n</sub>Ru(OOH)] being significantly higher than [L<sub>n</sub>Ru(OH<sub>2</sub>)]<sup>1+</sup>, which will favor the formation of  $[\{\text{L}_n\text{Ru}\}_2(\mu_{1,2}\text{-O}_2)]$  (step 6, Scheme 3B) over  $[\{\text{L}_n\text{Ru}\}_2(\mu\text{-OH})]^{1+}$  or  $[\{\text{L}_n\text{Ru}\}_2(\mu\text{-O})]$ . Furthermore, the greater Ru····Ru distance afforded by the μ<sub>1,2</sub>-O<sub>2</sub> bridging ligand will result in  $[\{\text{L}_n\text{Ru}\}_2(\mu_{1,2}\text{-O}_2)]$  being a lower energy species due to reduced steric clashing between L<sub>n</sub> sets compared to  $[\{\text{L}_n\text{Ru}\}_2(\mu\text{-OH})]^{1+}$  and  $[\{\text{L}_n\text{Ru}\}_2(\mu\text{-O})]$ , which feature shorter Ru····Ru distances due to the shorter μ-OH and μ-O bridging ligands.

Additionally, the formation of  $[\{\text{L}_n\text{Ru}\}_2(\mu_{1,2}\text{-O}_2)]$  offers a pathway through which **Ru1** can exhibit 1e<sup>-</sup> peroxidase-like reactivity without the Ru-containing species being irreversibly shunted off the dominant catalase cycle. Specifically, the peroxo

bond in  $\{[L_nRu]_2(\mu_{1,2}-O_2)\}$  can be reduced by 2 equiv. of ABTS<sup>2-</sup> and acquire 2 H<sup>+</sup> from the buffered solution to form 2 equiv. of  $[L_nRu-OH]$  (Scheme 3C). As shown in Scheme 3A,  $[L_nRu-OH]$  is an intermediate that participates in the catalase cycle.

In other complexes, moieties such as Ru-H, Ru-OOH, and Ru-O-O-Ru can exhibit characteristic features observable by <sup>1</sup>H NMR, IR, and Raman spectroscopy.<sup>50-55</sup> However, these techniques require mM concentrations (or higher), but **Ru1** has limited solubility (ca 1 mM) in water-miscible organic solvents. Furthermore, the **Ru1**-catalyzed H<sub>2</sub>O<sub>2</sub> disproportionation reaction shuts down when the volume % of H<sub>2</sub>O in the reaction solution drops below 70%. Thus, 300 μM is the highest **Ru1** concentration that can be achieved in aqueous solution that still affords catalytic H<sub>2</sub>O<sub>2</sub> disproportionation. We were unable to detect any Ru-H, Ru-OOH, or Ru-O-O-Ru intermediates (or any other **Ru1**-derived intermediates) in the **Ru1**-catalyzed H<sub>2</sub>O<sub>2</sub> disproportionation reaction using <sup>1</sup>H NMR, IR, and Raman spectroscopy, due to the inability to access analyte concentrations above 300 μM.

### Rate law derivation

To test the validity of the proposed mechanism for H<sub>2</sub>O<sub>2</sub> disproportionation catalyzed by **Ru1**, including the  $[L_nRu-OOH] \rightleftharpoons \{[L_nRu]_2(\mu_{1,2}-O_2)\}$  branch, we derived the general rate law and measured  $v_0$  as a function of  $[Ru1]_0$ ,  $[H_2O_2]_0$ , and  $[H^+]_0$ . Steps 1, 2, and 5 are relatively simple equilibria described by equilibrium constants  $K_1$ ,  $K_2$ , and  $K_5$ , respectively (Scheme 3A and 3B). From our prior mechanistic investigations of **Ru1**-catalyzed ABTS<sup>2-</sup> reduction with H<sub>2</sub>O<sub>2</sub>, we reasoned that elimination of O<sub>2</sub> from  $[L_nRu-OOH]$  (step 3, Scheme 3A) would be turnover-limiting and effectively irreversible ( $k_3 \ll k_4$  and  $k_3 \gg k_{-3}$ ). The pK<sub>a</sub> values reported for other  $[L_nRu-OH_2]^{1+}$  complexes range from 9-10, therefore we reasoned that protonation of  $L_nRu-OH$  to generate  $[L_nRu-OH_2]^{1+}$  (step 5, Scheme 3A) would be faster than the formation of  $L_nRu-OH$ , which would render step 4 effectively irreversible as well ( $k_5 \gg k_4$  and  $k_5 \gg k_{-4}$ ).

One turnover of the proposed catalytic cycle in Scheme 3A requires the consumption of 2 equiv. of H<sub>2</sub>O<sub>2</sub>, with the 1<sup>st</sup> equiv. being consumed during turnover-limiting formation of  $[L_nRu-H]$  (step 3) and the 2<sup>nd</sup> equiv. being consumed upon reaction with the  $[L_nRu-H]$  (step 4, Scheme 3A). The time-dependent change in  $[H_2O_2]$  can thus be described by Eqn. 1:

$$-\frac{d[H_2O_2]}{dt} = k_4[H_2O_2][RuH] \quad (1)$$

The time-dependent concentration of  $[L_nRu-H]$ , abbreviated as  $[RuH]$ , is unknown and cannot be measured directly. It is therefore necessary to express  $[RuH]$  as a function of known variables and constants. This expression can be determined using (i) the equilibrium equations for steps 1, 2, 5, and 6, (ii) the steady-state first-derivative equation for  $[RuH]$ , and (iii) the constraint that the sum of the concentrations of all Ru-containing species must be equal to  $[Ru1]_0$ . Using this approach, we can describe  $[RuH]$  as a function of  $[Ru1]_0$ ,  $[H_2O_2]_0$ , and  $[H^+]_0$ . However, the formation of  $\{[L_nRu]_2(\mu_{1,2}-O_2)\}$  (step 6, Scheme 3B)

introduces a non-linear term to the equation relating  $[Ru1]_0$  to  $[RuH]$ :

$$[Ru1]_0 = F_1 \cdot [RuH]^2 + F_2 \cdot [RuH] \quad (2)$$

The derivation of Eqn. 2 and the full expressions for  $F_1$ , a function of  $[H_2O_2]_0$ , and  $F_2$ , a function of both  $[H_2O_2]_0$  and  $[H^+]_0$ , can be found in the Supporting Information (Eqns. S1-S9). Because the expression for  $[Ru1]_0$  contains both  $[RuH]^2$  and  $[RuH]$  terms, solving for  $[RuH]$  requires using the quadratic equation (Eqns. S10-S13), which yields a non-linear relationship between  $[RuH]$  and  $[Ru1]_0$ :

$$[RuH] = \frac{-F_2 + \sqrt{F_2^2 + 4F_1 \cdot [Ru1]_0}}{2F_1} \quad (3)$$

The "±" operator in the numerator of Eqn. S12 simplifies to "+" in Eqn. 3 because equilibrium constants and rate constants cannot be negative, and thus having a "-" operator would have resulted in a negative value for  $[RuH]$ , which is impossible. Plugging Eqn. 3 into Eqn. 1 (Eqns. S14-S17) affords an expression (Eqn. 4) for the rate of H<sub>2</sub>O<sub>2</sub> consumption as a function of  $[Ru1]_0$ ,  $[H_2O_2]_0$ , and  $[H^+]_0$ , where  $G_1$  is a constant:

$$-\frac{d[H_2O_2]}{dt} = G_1 \cdot \left( -F_2 + \sqrt{F_2^2 + 4F_1 \cdot [Ru1]_0} \right) \quad (4)$$

Measuring the rate of H<sub>2</sub>O<sub>2</sub> consumption at very short times ( $v_0$ ) allows the time-dependent  $[H_2O_2]$  and  $[H^+]_0$  terms in  $F_1$  and  $F_2$  to be replaced with the known constants  $[H_2O_2]_0$  and  $[H^+]_0$ , respectively (Eqn. S18). By varying the initial concentration of only one of **Ru1**, H<sub>2</sub>O<sub>2</sub>, or H<sup>+</sup>, but holding the other two concentrations constant, Eqn. 3 simplifies to a single-variable function relating  $v_0$  (as the y-variable) to  $[Ru1]_0$ ,  $[H_2O_2]_0$ , or  $[H^+]_0$  (as the x-variable). If  $[Ru1]_0$  is varied but  $[H_2O_2]_0$ , or  $[H^+]_0$  are held constant (Eqns. S19-S22), the general rate law predicts the plot of  $v_0$  vs.  $[Ru1]_0$  will follow Eqn. 5. If  $[H_2O_2]_0$  is varied but  $[Ru1]_0$  and  $[H^+]_0$  are held constant (Eqns. S23-S26), the plot of  $v_0$  vs.  $[H_2O_2]_0$  will follow Eqn. 6. If  $[H^+]_0$  is varied but  $[Ru1]_0$  and  $[H_2O_2]_0$  are held constant (Eqns. S27-S30), the plot of  $v_0$  vs.  $[H_2O_2]_0$  will follow Eqn. 7. Note that  $a$ ,  $b$ , and  $c$  are constants in Eqns. 5-7 and  $[Ru1]_0$  is a constant in Eqn. 6-7.

$$y = (c)[-b + (b^2 + 4ax)^{1/2}] \quad (5)$$

$$y = (d)[-bx - c + \{(bx + c)^2 + 4a[Ru1]_0 \cdot x\}^{1/2}] \quad (6)$$

$$y = (d)[-bx - c + \{(bx + c)^2 + 4a[Ru1]_0\}^{1/2}] \quad (7)$$

### Analysis of reaction kinetics

To fit the experimental  $v_0$  vs.  $[Ru1]_0$  data and to not predict too high a rate of H<sub>2</sub>O<sub>2</sub> consumption in the absence of **Ru1**, Eqn. 5 should produce a trace that (i) has a more positive slope from  $[Ru1]_0 = 0$  to 10 μM than higher concentrations and (ii) increases

roughly linearly from  $[\text{Ru1}]_0 = 10$  to  $40 \mu\text{M}$ . An overlay of the Eqn. 5 trace (grey line, Figure 3A) on the plot of experimental  $v_0$  vs.  $[\text{Ru1}]_0$  data (black crosses, Figure 3A) shows that Eqn. 5 accurately describes the experimental data and satisfies the aforementioned constraints. If  $[\text{Ru1}]_0$  is very low, then  $[\text{L}_7\text{Ru}]_2(\mu_{1,2}\text{-O}_2)$  formation is negligible, and  $v_0$  increases with  $[\text{Ru1}]_0$  in roughly 1:1 fashion (i.e., the mechanism follows Scheme 3A with negligible contribution by Scheme 3B). As  $[\text{Ru1}]_0$  increases, more  $[\text{L}_7\text{Ru}]_2(\mu_{1,2}\text{-O}_2)$  forms, which decreases the relative amount of total Ru available to participate in the catalase cycle, and  $v_0$  increases with  $[\text{Ru1}]_0$  in less than 1:1 fashion (i.e., the mechanism follows a combination of the steps in Schemes 3A and 3B).

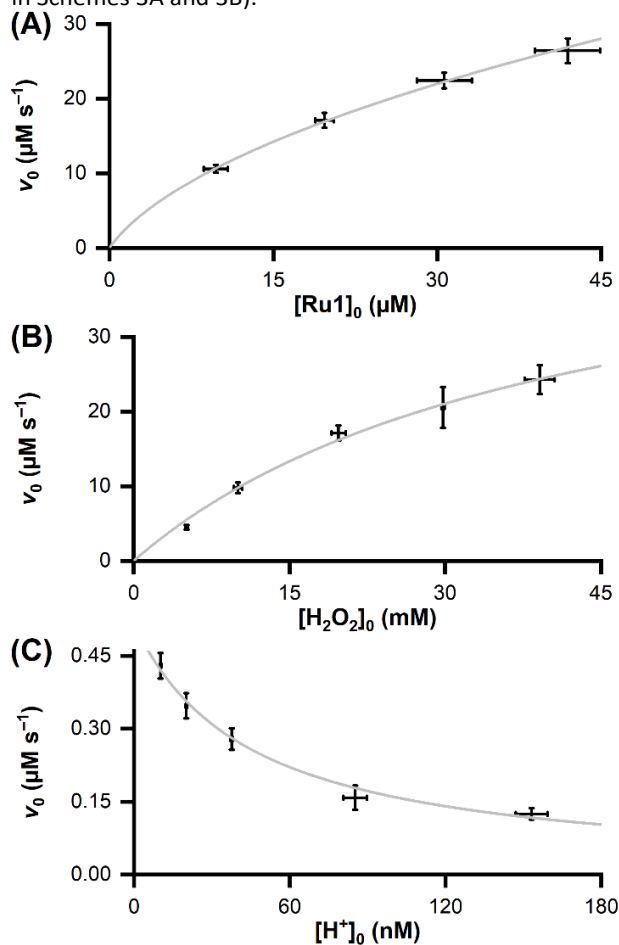


**Figure 3.** Dependence of the initial rate ( $v_0$ ) of **Ru1**-catalyzed  $\text{H}_2\text{O}_2$  disproportionation on (A)  $[\text{Ru1}]_0 = 10, 20, 30,$  or  $40 \mu\text{M}$ ; (B)  $[\text{H}_2\text{O}_2]_0 = 5, 10, 20, 30,$  or  $40 \text{ mM}$ ; (C)  $\text{pH} = 6.8, 7.1, 7.4, 7.7,$  or  $8.0$ . Conditions (unless specified otherwise):  $[\text{Ru1}]_0 = 20 \mu\text{M}$ ,  $[\text{H}_2\text{O}_2]_0 = 20 \text{ mM}$ , PBS ( $\text{pH} 7.4$ ),  $25^\circ\text{C}$ .

The plot of  $v_0$  vs.  $[\text{H}_2\text{O}_2]_0$  (Figure 3B) shows  $v_0$  increasing with increasing  $[\text{H}_2\text{O}_2]_0$ , but with a shallower slope at higher  $[\text{H}_2\text{O}_2]_0$  values, behavior which can be accurately modeled by Eqn. 6. The shallower slope at higher  $[\text{H}_2\text{O}_2]_0$  reflects the fact that  $\text{H}_2\text{O}_2$  coordinates to Ru before the turnover-limiting step (i.e., step 1, Scheme 3A). At sufficiently high  $[\text{H}_2\text{O}_2]$ , the equilibrium in step 1 saturates and  $v_0$  cannot increase any further.

Conversely,  $v_0$  decreases as  $[\text{H}^+]_0$  increases, with the slope shallower at higher  $[\text{H}^+]_0$  values (Figure 3C), whereby the

variation in the  $v_0$  vs.  $[\text{H}^+]_0$  experimental data can be accurately modeled by Eqn. 7. The general trend of greater  $v_0$  values at lower  $[\text{H}^+]_0$  arises because  $\text{H}^+$  dissociation must occur (step 2, Scheme 3A) before the turnover-limiting step (step 3, Scheme 3A). The diminishing impact of increasing  $[\text{H}^+]_0$  on  $v_0$  at higher values reflects the fact that step 2 is an equilibrium process.

Although the rate law equations that describe the  $[\text{H}_2\text{O}_2]_0$  and  $[\text{H}^+]_0$  dependencies of **Ru1**-catalyzed  $\text{H}_2\text{O}_2$  disproportionation differ significantly from **Ru1**-catalyzed  $\text{ABTS}^{\bullet-}$  reduction with  $\text{H}_2\text{O}_2$ , the general trends are similar, which suggests that the mechanism for the former reaction is partially conserved with the latter. The most noteworthy difference is that **Ru1** does catalyze  $\text{H}_2\text{O}_2$  disproportionation in pure  $\text{H}_2\text{O}$ , but **Ru1** cannot catalyze  $\text{ABTS}^{\bullet-}$  reduction with  $\text{H}_2\text{O}_2$  in pure  $\text{H}_2\text{O}$ . The origin of this is that **Ru1**-catalyzed  $\text{ABTS}^{\bullet-}$  reduction with  $\text{H}_2\text{O}_2$  generates a net 2 equiv. of  $\text{H}^+$  from each turnover of the catalytic cycle. A lack of buffer would mean that the  $\text{H}^+$  released would decrease the pH of the reaction solution to the point that the rate of **Ru1**-catalyzed  $\text{ABTS}^{\bullet-}$  reduction with  $\text{H}_2\text{O}_2$  becomes negligible. In contrast, **Ru1**-catalyzed  $\text{H}_2\text{O}_2$  disproportionation releases 1 equiv. of  $\text{H}^+$  to solution in step 2 (Scheme 3A), but then acquires 1 equiv. of  $\text{H}^+$  from solution in step 5, with no net  $\text{H}^+$  generation or consumption during catalytic cycle turnover.

Eyring–Polanyi analysis of **Ru1**-catalyzed  $\text{H}_2\text{O}_2$  disproportionation rate data collected at  $T = 20, 25, 30,$  and  $35^\circ\text{C}$  (Figure 4) reveal that  $\Delta H^\ddagger = 13.6 \pm 0.7 \text{ kcal mol}^{-1}$  and  $\Delta S^\ddagger = -26.1 \pm 2.4 \text{ cal mol}^{-1} \text{ K}^{-1}$ . For comparison, **Ru1**-catalyzed  $\text{ABTS}^{\bullet-}$  reduction with  $\text{H}_2\text{O}_2$  exhibits  $\Delta H^\ddagger = 29.1 \pm 0.6 \text{ kcal mol}^{-1}$  and  $\Delta S^\ddagger = 25.5 \pm 1.9 \text{ cal mol}^{-1} \text{ K}^{-1}$ . Notably, the  $\Delta S^\ddagger$  value for **Ru1**-catalyzed  $\text{H}_2\text{O}_2$  disproportionation is comparable in magnitude but opposite in sign to the value for **Ru1**-catalyzed  $\text{ABTS}^{\bullet-}$  reduction with  $\text{H}_2\text{O}_2$ , which indicates significant differences in transition state structures and properties. Indeed, all our previous studies of **Ru1**-catalyzed  $\text{ABTS}^{\bullet-}$  reduction, with any terminal reductant, revealed positive  $\Delta S^\ddagger$  values.

A large, negative  $\Delta S^\ddagger$  value for **Ru1**-catalyzed  $\text{H}_2\text{O}_2$  disproportionation can be rationalized by the reaction of the Ru–H intermediate with  $\text{H}_2\text{O}_2$  (step 4, Scheme 3A). Because one OH group from  $\text{H}_2\text{O}_2$  is transferred to Ru to yield the Ru–OH intermediate, then the corresponding transition state most likely features an associative interaction between  $\text{H}_2\text{O}_2$  and Ru–H, potentially including H-bonding or direct coordination, which would give rise to the large, negative  $\Delta S^\ddagger$  value for **Ru1**-catalyzed  $\text{H}_2\text{O}_2$  disproportionation. In contrast, the reaction of the Ru–H intermediate with  $\text{ABTS}^{\bullet-}$  in **Ru1**-catalyzed  $\text{ABTS}^{\bullet-}$  reduction with  $\text{H}_2\text{O}_2$  involves  $1e^-$  transfer from Ru–H to  $\text{ABTS}^{\bullet-}$ . A large, positive  $\Delta S^\ddagger$  value for this process suggests outer-sphere electron transfer and coupling to the preceding step, fragmentation of Ru–OOH into Ru–H and  $\text{O}_2$ . The larger, positive  $\Delta H^\ddagger$  value for **Ru1**-catalyzed  $\text{ABTS}^{\bullet-}$  reduction with  $\text{H}_2\text{O}_2$  likely reflects the fact that a negatively-charged electron must be removed from a neutral Ru–H intermediate and separated from the resulting cationic species, and then must be transferred to an already negatively-charged  $\text{ABTS}^{\bullet-}$  molecule, both of which are energetically-unfavorable due to Coulombic effects. In contrast, both  $\text{H}_2\text{O}_2$  and the Ru–H intermediate are neutral, therefore unfavorable Coulombic effects are absent.

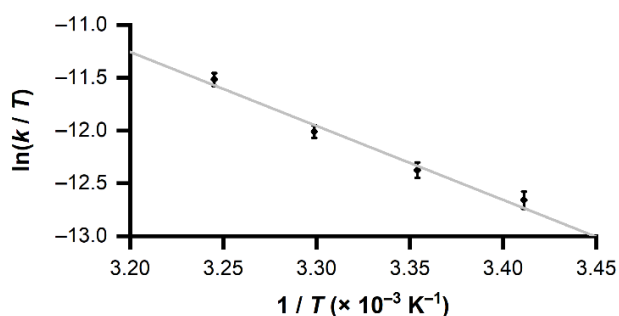


Figure 4. Eyring–Polanyi plot of  $\ln(k/T)$  vs.  $1/T$  at  $T = 20, 25, 30,$  and  $35$  °C. Conditions:  $[\text{Ru}1]_0 = 20$   $\mu\text{M}$ ,  $[\text{H}_2\text{O}_2]_0 = 20$  mM, PBS (pH 7.4).

## Conclusions

This report constitutes to the best of our knowledge the first instance of an organometallic complex that functions as a catalase mimic (i.e., catalyzes the reaction  $\text{H}_2\text{O}_2 \rightarrow \text{H}_2\text{O} + \frac{1}{2} \text{O}_2$ ), which is surprising given that catalytic  $\text{H}_2\text{O}_2$  disproportionation has been reported for a multitude of non-organometallic complexes comprising a wide variety of metals.<sup>56–63</sup> A similarly rich diversity of peroxidase model complexes also exists.<sup>64–72</sup>

Compared to existing redox therapeutics, the Mn–porphyrin and –salen complexes initially developed to mimic MnSOD, **Ru1** exhibits dramatically higher catalase activity,  $\text{H}_2\text{O}_2$  stability, and catalase/peroxidase selectivity than the highest individual values reported for the MnSOD mimics (11.9-, 120-, and 89.2-fold greater, respectively). When these values are aggregated for each complex, the overall performance of **Ru1** as a catalase mimic is 4 orders of magnitude superior to any Mn–porphyrin or –salen biomimetic complex.

A major focus area of research involving Ru complexes in living systems is harnessing their cytotoxic effects for anticancer applications,<sup>73–81</sup> but there is some evidence that Ru complexes can harm or kill non-cancer cells.<sup>82</sup> Interestingly, one report describes a non-organometallic Ru complex with anticancer effects that inhibits the activities of endogenous catalases.<sup>83</sup> Preliminary studies of **Ru1** in RAW 264.7 cells revealed that concentrations of **Ru1** up to 100  $\mu\text{M}$  are non-cytotoxic.

Given that the catalase activity of **Ru1** is nearly 9000-fold faster than its peroxidase activity, its reactivity as a redox therapeutic will be almost exclusively antioxidant, with minimal pro-oxidant reactivity. This selectivity will significantly decrease uncertainty when investigating the behavior of **Ru1** in biological systems. Furthermore, the much greater catalase activity and  $\text{H}_2\text{O}_2$  stability of **Ru1** will enable it to alleviate significantly more severe and longer lasting oxidative stress in living systems than current Mn–porphyrin or Mn–salen complexes. The ability of **Ru1** to prevent or alleviate biological oxidative stress will be detailed in a subsequent report.

## Conflicts of interest

There are no conflicts to declare.

## Acknowledgements

This work was supported by the US National Science Foundation (DMR-1555224). We thank Dr. Yamin Htet for prior work with **Ru1** and for helpful discussions.

## Notes and references

- P. Chelikani, I. Fita and P. C. Loewen, *Cell. Mol. Life Sci.*, 2004, **61**, 192–208.
- H.-P. Hersleth, U. Ryde, P. Rydberg, C. H. Görbitz and K. K. Andersson, *J. Inorg. Biochem.*, 2006, **100**, 460–476.
- M. Zámocký, S. Hofbauer, I. Schaffner, B. Gasselhuber, A. Nicolussi, M. Soudi, K. F. Pirker, P. G. Furtmüller and C. Obinger, *Arch. Biochem. Biophys.*, 2015, **574**, 108–119.
- D. W. S. Wong, *Appl. Biochem. Biotechnol.*, 2009, **157**, 174–209.
- T. Ishikawa and S. Shigeoka, *Biosci. Biotechnol. Biochem.*, 2008, **72**, 1143–1154.
- J. E. Erman and L. B. Vitello, *Biochim. Biophys. Acta*, 2002, **1597**, 193–220.
- L. S. Harman, D. K. Carver, J. Schreiber and R. P. Mason, *J. Biol. Chem.*, 1986, **261**, 1642–1648.
- C. Delporte, K. Z. Boudjeltia, P. G. Furtmüller, R. A. Maki, M. Dieu, C. Noyon, M. Soudi, D. Dufour, C. Coremans, V. Nuyens, F. Reye, A. Rousseau, M. Raes, N. Moguilevsky, M. Vanhaeverbeek, J. Ducobu, J. Nève, B. Robaye, L. Vanhamme, W. F. Reynolds, C. Obinger and P. V. Antwerpen, *J. Biol. Chem.*, 2018, **293**, 6374–6386.
- A. Taurog, M. L. Dorris and D. R. Doerge, *Arch. Biochem. Biophys.*, 1996, **330**, 24–32.
- M. Hofrichter and R. Ullrich, *Appl. Microbiol. Biotechnol.*, 2006, **71**, 276–288.
- R. Z. Harris, S. Newmyer and P. R. Ortiz de Montellano, *J. Biol. Chem.*, 1993, **268**, 1637–1645.
- H. N. Kirkman and G. F. Gaetani, *Trends Biochem. Sci.*, 2007, **32**, 44–50.
- J. Vlasits, C. Jakopitsch, M. Bernroither, M. Zamocky, P. G. Furtmüller and C. Obinger, *Arch. Biochem. Biophys.*, 2010, **500**, 74–81.
- I. Batinić-Haberle, A. Tovmasyan and I. Spasojević, *Redox Biol.*, 2015, **5**, 43–65.
- I. Batinić-Haberle, A. Tovmasyan, E. R. H. Roberts, Z. Vujaskovic, K. W. Leong and I. Spasojević, *Antiox. Redox Signal.*, 2014, **20**, 2372–2415.
- S. Miriyala, I. Spasojević, A. Tovmasyan, D. Salvemini, Z. Vujaskovic, D. St. Clair and I. Batinić-Haberle, *Biochim. Biophys. Acta*, 2012, **1822**, 794–814.
- I. Batinić-Haberle, Z. Rajic, A. Tovmasyan, J. S. Rebouças, X. Ye, K. W. Leong, M. W. Dewhirst, Z. Vujaskovic, L. Benov and I. Spasojević, *Free Radic. Biol. Med.*, 2011, **51**, 1035–1053.
- I. Batinić-Haberle, J. S. Rebouças and I. Spasojević, *Antiox. Redox Signal.*, 2010, **13**, 877–918.
- R. A. Rosenthal, K. D. Huffman, L. W. Fiset, C. A. Dampousse, W. B. Callaway, B. Malfroy and S. R. Doctrow, *J. Biol. Inorg. Chem.*, 2009, **14**, 979–991.
- A. Tovmasyan, C. G. C. Maia, T. Weitner, S. Carballal, R. S. Sampaio, D. Lieb, R. Ghazaryan, I. Ivanovic-Burmazovic, G. Ferrer-Sueta, R. Radi, J. S. Rebouças, I. Spasojević, L. Benov and I. Batinić-Haberle, *Free Radic. Biol. Med.*, 2015, **86**, 308–321.

21. , All potentials are reported relative to NHE unless specified otherwise.
22. P. M. Wood, *Biochem. J.*, 1988, **253**, 287–289.
23. D. K. Ali, M. Oriowo, A. Tovmasyan, I. Batinic-Haberle and L. Benov, *Redox Biol.*, 2013, **1**, 457–466.
24. J.-Y. Liu, X.-F. Li, Z.-X. Guo, Y.-Z. Li, A.-J. Huang and W.-B. Chang, *J. Mol. Catal. A*, 2002, **179**, 27–33.
25. R. Kubota, T. Takabe, K. Arima, H. Taniguchi, S. Asayama and H. Kawakami, *J. Mater. Chem. B*, 2018, **6**, 7050–7059.
26. A. Squarcina, A. Sorarù, F. Rigodanza, M. Carraro, G. Brancatelli, T. Carofiglio, S. Geremia, V. Larosa, T. Morosinotto and M. Bonchio, *ACS Catal.*, 2017, **7**, 1971–1976.
27. Y. Noritake, N. Umezawa, N. Kato and T. Higuchi, *Inorg. Chem.*, 2013, **52**, 3653–3662.
28. S. Meftah and R. Yazdanparast, *Iran. J. Chem. Chem. Eng.*, 2013, **32**, 67–75.
29. V. Oliveri, A. Puglisi and G. Vecchio, *Dalton Trans.*, 2011, **40**, 2913–2919.
30. N. Umezawa, N. Matsumoto, S. Iwama, N. Kato and T. Higuchi, *Bioorg. Med. Chem.*, 2010, **18**, 6340–6350.
31. V. Lanza and G. Vecchio, *J. Inorg. Biochem.*, 2009, **103**, 381–388.
32. S. R. Doctrow, K. Huffman, C. B. Marcus, G. Tocco, E. Malfroy, C. A. Adinolfi, H. Kruk, K. Baker, N. Lazarowych, J. Mascarenhas and B. Malfroy, *J. Med. Chem.*, 2002, **45**, 4549–4558.
33. W.-T. Lee, S. Xu, D. A. Dickie and J. M. Smith, *Eur. J. Inorg. Chem.*, 2013, 3867–3873.
34. W.-T. Lee, S. B. Muñoz, D. A. Dickie and J. M. Smith, *Angew. Chem. Int. Ed.*, 2014, **53**, 9856–9859.
35. A. Flórido, N. Saraiva, S. Cerqueira, N. Almeida, M. Parsons, I. Batinic-Haberle, J. P. Miranda, J. G. Costa, G. Carrara, M. Castro, N. G. Oliveira and A. S. Fernandes, *Redox Biol.*, 2019, **20**, 367–378.
36. Y. Yulyana, A. Tovmasyan, I. A. W. Ho, K. C. Sia, J. P. Newman, W. H. Ng, C. M. Guo, K. M. Hui, I. Batinic-Haberle and P. Y. P. Lam, *Stem Cell Rev. Rep.*, 2016, **12**, 140–155.
37. I. Batinic-Haberle, A. Tovmasyan and I. Spasojevic, *Antiox. Redox Signal.*, 2018, **29**, 1691–1724.
38. Z. Rajic, A. Tovmasyan, O. L. de Santana, I. N. Peixoto, I. Spasojevic, S. A. do Monte, E. Ventura, J. S. Rebouças and I. Batinic-Haberle, *J. Inorg. Biochem.*, 2017, **169**, 50–60.
39. Y. Htet and A. G. Tennyson, *J. Am. Chem. Soc.*, 2016, **138**, 15833–15836.
40. Y. Htet and A. G. Tennyson, *Angew. Chem. Int. Ed.*, 2016, **55**, 8556–8560.
41. Y. Htet and A. G. Tennyson, *Chem. Sci.*, 2016, **7**, 4052–4058.
42. Y. Htet, Z. Lu, S. A. Trauger and A. G. Tennyson, *Chem. Sci.*, 2019, **10**, 2025–2033.
43. S. L. Scott, W.-J. Chen, A. Bakac and J. H. Espenson, *J. Phys. Chem.*, 1993, **97**, 6710–6714.
44. , Although catalytic H<sub>2</sub>O<sub>2</sub> disproportionation has been reported for a wider variety of synthetic complexes than just Mn–porphyrin and Mn–salen complexes, detailed comparisons and discussion are only possible with MnSOD mimics for which both catalase and peroxidase reaction kinetic data are available.
45. , Values of  $v_0$  are calculated from the slopes of the [H<sub>2</sub>O<sub>2</sub>] vs.  $t$  plots at  $t_0'$ , where  $t_0'$  was identified as the time at which the first-derivatives of the [H<sub>2</sub>O<sub>2</sub>] vs.  $t$  plots reached a minimum. Typically,  $t_0'$  occurred <4 min after H<sub>2</sub>O<sub>2</sub> addition and when <10% of H<sub>2</sub>O<sub>2</sub> had been consumed.
46. , To be consistent with the reported kinetics for the Mn–porphyrin and Mn–salen complexes, catalase TOF values for **Ru1** in units of s<sup>-1</sup> were calculated by dividing the initial rate of H<sub>2</sub>O<sub>2</sub> consumption in μM s<sup>-1</sup> by the concentration of **Ru1** in μM.
47. , In this manuscript, catalase TOF and peroxidase TOF refer specifically to H<sub>2</sub>O<sub>2</sub> consumption. Literature values for O<sub>2</sub> production and ABTS<sup>•+</sup> production can be converted to H<sub>2</sub>O<sub>2</sub> consumption via multiplication by 2 and 0.5, respectively.
48. R. Re, N. Pellegrini, A. Proteggente, A. Pannala, M. Yang and C. Rice-Evans, *Free Radic. Biol. Med.*, 1999, **26**, 1231–1237.
49. , There is dramatic variation in the catalase reaction kinetics reported for many Mn–salen complexes. There are even with instances of the same research group studying the same complex a second time and obtaining a second catalase TOF more than 10-fold lower than the TOF in the initial report. Fortunately, each report on Mn–salen complexes used for comparison to **Ru11** included at least one Mn–salen complex that had been measured more than once. Dividing the corrected second value by the value in the initial report afforded a correction factor that was applied to each catalase TOF value.
50. M. Takenaka, M. Kikkawa, T. Matsumoto, T. Yatabe, T. Ando, K.-S. Yoon and S. Ogo, *Chem. Asian J.*, 2018, **13**, 3180–3184.
51. G. A. Silantsev, O. A. Filippov, P. M. Tolstoy, N. V. Belkova, L. M. Epstein, K. Weisz and E. S. Shubina, *Inorg. Chem.*, 2013, **52**, 1787–1797.
52. T. A. Tronic, W. Kaminsky, M. K. Coggins and J. M. Mayer, *Inorg. Chem.*, 2012, **51**, 10916–10928.
53. L. J. L. Häller, E. Mas-Marzá, A. Moreno, J. P. Lowe, S. A. Macgregor, M. F. Mahon, P. S. Pregosin and M. K. Whittlesey, *J. Am. Chem. Soc.*, 2009, **131**, 9618–9619.
54. J. Matthes, S. Gründemann, A. Toner, Y. Guari, B. Donnadiou, J. Spandl, S. Sabo-Etienne, E. Clot, H.-H. Limbach and B. Chaudret, *Organometallics*, 2004, **23**, 1424–1433.
55. M. Tamm, A. Kunst, F. E. Hahn, T. Pape and R. Fröhlich, *Z. Anorg. Allg. Chem.*, 2003, **629**, 2408–2414.
56. A. J. Ingram, K. L. Walker, R. N. Zare and R. M. Waymouth, *J. Am. Chem. Soc.*, 2015, **137**, 13632–13646.
57. S. K. Chatterjee, R. C. Maji, S. K. Barman, M. M. Olmstead and A. K. Patra, *Angew. Chem. Int. Ed.*, 2014, **53**, 10184–10189.
58. I. Schepetkin, A. Potapov, A. Khlebnikov, E. Korotkova, A. Lukina, G. Malovichko, L. Kirpotina and M. T. Quinn, *J. Biol. Inorg. Chem.*, 2006, **11**, 499–513.
59. J. Gao, A. E. Martell and J. H. Reibenspies, *Inorg. Chim. Acta*, 2003, **346**, 32–42.
60. R. Bandyopadhyay, S. K. Maiti and R. Bhattacharyya, *Inorg. Chem. Commun.*, 2002, **5**, 259–263.
61. Y. M. Goh and W. Nam, *Inorg. Chem.*, 1998, **38**, 914–920.
62. S. Ménage, J. M. Vincent, C. Lambeaux and M. Fontecave, *J. Chem. Soc., Dalton Trans.*, 1994, 2081–2084.
63. J. M. Aubry and B. Cazin, *Inorg. Chem.*, 1988, **27**, 2013–2014.
64. A. M. Aslam, S. Rajagopal, M. Vairamani and M. Ravikumar, *Transition Met. Chem.*, 2011, **36**, 751–759.

65. H. Biava and S. Signorella, *Polyhedron*, 2010, **29**, 1001–1006.
66. P. Wu, C. Çelik, G. Santoni, J. Dallery and D. Rehder, *Eur. J. Inorg. Chem.*, 2008, **2008**, 5203–5213.
67. S. Tabassum, S. Parveen and F. Arjmand, *Transition Met. Chem.*, 2005, **30**, 196–204.
68. A. G. J. Ligtenbarg, R. Hage and B. L. Feringa, *Coord. Chem. Rev.*, 2003, **237**, 89–101.
69. H. Fujii, *Coord. Chem. Rev.*, 2002, **226**, 51–60.
70. I. Bernal, I. M. Jensen, K. B. Jensen, C. J. McKenzie, H. Toftlund and J.-P. Tuchagues, *J. Chem. Soc., Dalton Trans.*, 1995, 3667–3675.
71. D. Mandon, R. Weiss, K. Jayaraj, A. Gold, J. Turner, E. Bill and A. X. Trautwein, *Inorg. Chem.*, 1992, **31**, 4404–4409.
72. J. T. Groves, R. C. Haushalter, M. Nakamura, T. E. Nemo and B. J. Evans, *J. Am. Chem. Soc.*, 1981, **103**, 2884–2886.
73. C. Li, K.-W. Ip, W.-L. Man, D. Song, M.-L. He, S.-M. Yiu, T.-C. Lau and G. Zhu, *Chem. Sci.*, 2017, **8**, 6868–6870.
74. L.-m. Chen, F. Peng, G.-d. Li, X.-m. Jie, K.-r. Cai, C. Cai, Y. Zhong, H. Zeng, W. Li, Z. Zhang and J.-c. Chen, *J. Inorg. Biochem.*, 2016, **156**, 64–74.
75. T. S. Morais, F. C. Santos, T. F. Jorge, L. Côrte-Real, P. J. A. Madeira, F. Marques, M. P. Robalo, A. Matos, I. Santos and M. H. Garcia, *J. Inorg. Biochem.*, 2014, **130**, 1–14.
76. A. M. Palmer, B. Peña, R. B. Sears, O. Chen, M. E. Ojaimi, R. P. Thummel, K. R. Dunbar and C. Turro, *Phil. Trans. R. Soc. A*, 2013, **371**, 20120135.
77. G.-J. Lin, G.-B. Jiang, Y.-Y. Xie, H.-L. Huang, Z.-H. Liang and Y.-J. Liu, *J. Biol. Inorg. Chem.*, 2013, **18**, 873–882.
78. M. A. Sgambellone, A. David, R. N. Garner, K. R. Dunbar and C. Turro, *J. Am. Chem. Soc.*, 2013, **135**, 11274–11282.
79. M. Auzias, B. Therrien, G. Süß-Fink, P. Štěpnička, W. H. Ang and P. J. Dyson, *Inorg. Chem.*, 2008, **47**, 578–583.
80. A. Habtemariam, M. Melchart, R. Fernández, S. Parsons, I. D. H. Oswald, A. Parkin, F. P. A. Fabbiani, J. E. Davidson, A. Dawson, R. E. Aird, D. I. Jodrell and P. J. Sadler, *J. Med. Chem.*, 2006, **49**, 6858–6868.
81. D. N. Akbayeva, L. Gonsalvi, W. Oberhauser, M. Peruzzini, F. Vizza, P. Brüggeller, A. Romerosa, G. Savad and A. Bergamo, *Chem. Commun.*, 2003, 264–265.
82. P. Hu, Y. Wang, Y. Zhang, H. Song, F. Gao, H. Lin, Z. Wang, L. Wei and F. Yang, *RSC Adv.*, 2016, **6**, 29963–29976.
83. B. S. Demir, T. Keleş and O. Serindağ, *Bioinorg. Chem. Appl.*, 2014, **2014**, Article ID 717421.